Open Access
Full Paper
Journal of Agricultural Meteorology 82(3): 138–150, 2026

Regional and topographic controls on strong nocturnal cooling in Hokkaido, Japan

Tsutomu WATANABE[a,†], Misa YAMANOUCHI[b], Masayuki KAWASHIMA[a] and Kou SHIMOYAMA[a]

([a] Institute of Low Temperature Science, Hokkaido University, Kita 19 Nishi 8, Kita-ku, Sapporo 060-0819, Japan
[b] Graduate School of Environmental Science, Hokkaido University, Kita 10 Nish 5, Kita-ku, Sapporo 060-0810, Japan)

Abstract

Winter nocturnal temperature drops in cold regions arise from complex interactions between radiative cooling and terrain-induced micrometeorological processes. Using long-term operational surface observations from 1978 to 2025, this study investigated the regional and topographic controls on nocturnal cooling in Hokkaido, Japan. The results revealed a pronounced regional contrast in long-term mean temperature drops, with stronger cooling on the Pacific side and weaker cooling on the Sea of Japan side. These differences reflect variations in nocturnal radiative conditions, inferred indirectly from the sunshine duration during the 24-h noon-to-noon period, and are further modulated by local cold-air pooling characteristics, as represented by clear-night wind speed. With respect to extreme temperature drops, principal component analysis identified southeastern and northern Hokkaido as the regions most susceptible to intense and widespread nocturnal cooling. A key contribution of this study is the introduction of two terrain-based metrics that capture the terrain characteristics responsible for such large temperature drops, extending the analysis beyond the basin- and valley-focused approaches common in previous studies. These metrics are R_{av}, the area–volume ratio representing the radiative-cooling capacity of the surrounding terrain, and A_{site}/A_{in}, the fraction of the inner-catchment area lying below the site elevation, representing terrain openness and the site's relative elevation. Analysis indicated that cooling in shallow terrain is governed primarily by R_{av}, whereas cooling in deep terrain depends on the cold-air pooling structure and the site's relative position within the pool, captured by A_{site}/A_{in}. Both metrics are physically interpretable and rely solely on digital elevation data, making them broadly applicable to other cold regions. These findings provide a unified and mechanistically grounded framework for understanding extreme nocturnal cooling across diverse terrain types and offer practical tools for identifying areas vulnerable to extreme low temperatures in cold-region agriculture and forest management.

Key words: Cold-air pooling, Extreme cold, Nocturnal temperature drop, Radiative cooling, Terrain effects

1. Introduction

Winter nocturnal temperature drops in cold regions are governed both by radiative cooling and by interactions between the atmosphere and the underlying terrain. Under clear and calm conditions, longwave radiative loss from the surface promotes the development of strong surface-based temperature inversions, leading to extremely low near-surface temperatures. These processes are particularly important in complex terrain, where cold-air pooling (CAP), drainage flows, and terrain-induced wind patterns interact to shape the local thermal environment. A comprehensive understanding of these processes is essential for advancing micrometeorology in diverse topographic settings and for assessing low-temperature hazards affecting agricultural and forest ecosystems.

Extreme nocturnal cooling has important implications for agricultural production. Wintertime minimum temperatures influence the overwintering survival of perennial crops, causing frost and freeze damage to fruit trees (Snyder and Melo-Abreu, 2005) and leading to severe freeze injury and winterkill in perennial forage grasses (Thivierge *et al*., 2023). Livestock housed in unheated or partially heated facilities are likewise susceptible to thermal stress during severe cold events (Debnath *et al*., 2024). Cold-region environments also provide natural cooling resources for temperature-sensitive infrastructure. Snow, ice, and cold air have been widely utilized for renewable cooling applications in cold-climate regions, including low-energy cooling of agricultural and industrial storage facilities, snow- and ice-based building cooling systems, and free-air or snow-assisted cooling in data centers (Kimura *et al*., 2010; Hamada *et al*., 2007, 2012; Tsuda *et al*., 2015; Yan *et al*., 2016; Tareen *et al*., 2024). In Hokkaido (Japan), the spatial distribution of natural cold-energy resources—including snow, ice, and frozen soil—has been systematically classified to demonstrate the region's strong potential for renewable cold-energy utilization (Kimura and Urano, 2005). Collectively, these examples highlight the broader societal relevance of cold-region climate processes and underscore the need to identify the key processes that govern extreme nocturnal cooling.

A central factor underlying these diverse impacts and applications is the strong influence of terrain on nocturnal cooling. Terrain geometry plays a fundamental role in controlling the formation and persistence of CAP. Terrain depth and basin enclosure affect the accumulation of cold air in depressions, with

Received; February 26, 2026
Accepted; June 10, 2026
[†]Corresponding author: t-wata@lowtem.hokudai.ac.jp
DOI: 10.2480/agrmet.D-26-00004

deeper and more enclosed basins exhibiting thicker inversion layers. Observational and numerical studies in Japan have shown that valley depth, basin shape, and ridge height strongly influence the magnitude of nocturnal cooling (Kondo and Kuwagata, 1984; Kondo *et al*., 1989; Kondo and Okusa, 1990). Thermally driven downslope flows further modulate nocturnal temperature minima by transporting cooled air from surrounding slopes into valley floors (Zardi and Whiteman, 2013). These processes have been documented across diverse environments, including alpine valleys in the European Alps (Dorninger *et al*., 2011), Scandinavian valleys (Gustavsson *et al*., 1998), a semi-closed desert basin in Chile (Flores *et al*., 2020), and inland undulating terrain in central Japan (Kimura *et al*., 2023), as well as snow-covered plains in eastern Hokkaido, where strong nocturnal cooling frequently develops under weak-wind conditions (Yazaki *et al*., 2017).

Despite these advances, most previous related studies focused on basins, valleys, and other strongly confined terrain where CAP is most pronounced. In contrast, much less is known about how nocturnal cooling operates across a broader spectrum of terrain types, including gentle undulations, open plains, shallow lowlands, and weakly confined depressions. Although several studies attempted to use topographic indicators to identify locations within complex terrain where strong CAP is likely to develop (McKee and O'Neal, 1989; Lindkvist *et al*., 2000; Chung *et al*., 2006; Lundquist *et al*., 2008; Kimura *et al*., 2023), such efforts generally focused on valley terrain within relatively narrow geographic areas. Consequently, the topographic controls on cooling intensity across broader and more diverse terrain settings remain poorly characterized. This knowledge gap limits our ability to interpret and predict regional patterns of nocturnal cooling and to assess their implications for agricultural and forest ecosystems, as well as for emerging applications such as renewable cold-energy utilization.

Hokkaido, Japan's northernmost island, provides an ideal setting for addressing this knowledge gap. Its large-scale topography produces pronounced regional contrasts in winter weather, and the island encompasses a wide variety of terrain types, from extensive plains to deep basins. Hokkaido experiences the lowest winter temperatures in Japan, further highlighting its suitability for examining extreme nocturnal cooling. These features enable systematic investigation of how terrain influences nocturnal cooling across diverse landscape configurations. Although CAP-related processes have been examined in previous related research (e.g., Maki *et al*., 1984, 1986; Kondo *et al*., 1983, 1989), few studies have explored their long-term, region-wide patterns using operational meteorological observations.

In this study, we analyzed long-term surface meteorological observations collected across Hokkaido during January and February from 1978 to 2025 to clarify the regional characteristics of nocturnal temperature drops. We identified the dominant meteorological factors controlling spatial variability, introduced terrain-based metrics to quantify radiative-cooling capacity, and evaluated their relevance across diverse terrain types. The findings of this study provide a unified framework for understanding extreme nocturnal cooling in complex terrain and offer insights relevant to agricultural risk assessment, forest-ecosystem management, and cold-region climate adaptation strategies.

2. Materials and methods

2.1. Study area and winter climate

Hokkaido exhibits a pronounced east–west climatic contrast shaped by its complex topography, including the Ishikari and Hidaka Mountains, which reach elevations of approximately 2000 m (Fig. 1). Long-term climatological averages of temperature, precipitation, and snow depth differ markedly between the Pacific side and the Sea of Japan side of the island. During winter, frequent cold-air outbreaks from Siberia generate strong northwesterly winds. As a result, the western–northern regions facing the Sea of Japan experience persistent cloud cover and frequent snowfall, whereas the southeastern Pacific side is characterized by more frequent clear-sky conditions. Although snow depths vary across inland areas, most of Hokkaido remains continuously snow-covered throughout winter. Thus, aside from urban areas and some coastal zones with relatively shallow snow cover, spatial variability in wintertime surface conditions is generally limited.

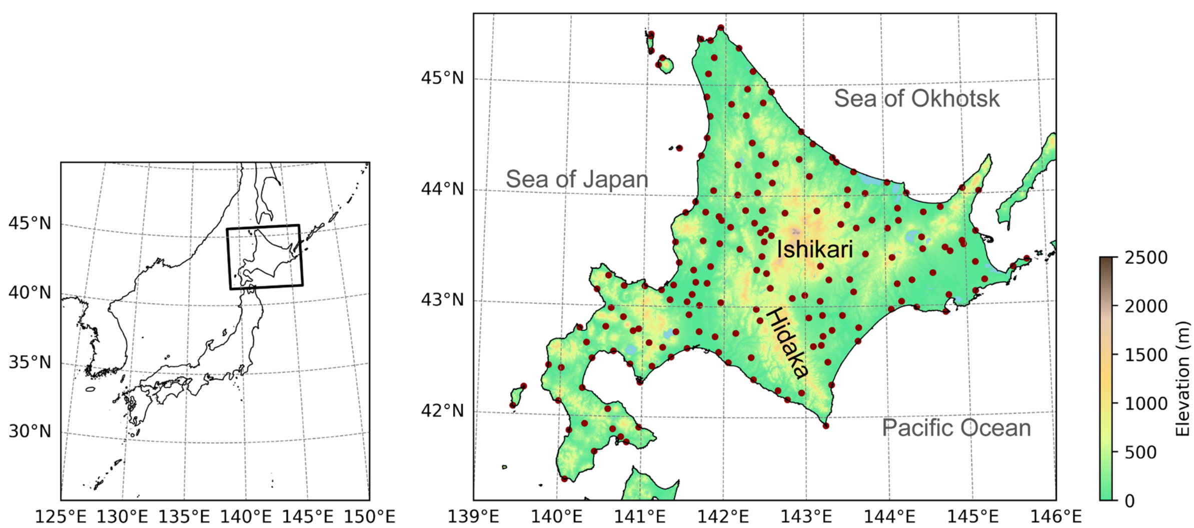

Fig. 1. Map of the study area, with dots indicating the locations of AMeDAS sites.

2.2. Meteorological data

Surface meteorological data collected by the Automated Meteorological Data Acquisition System (AMeDAS), operated by the Japan Meteorological Agency, were used in this study. The analysis employed daily and hourly observations of air temperature, wind speed, and sunshine duration acquired from 178 AMeDAS sites across Hokkaido (site locations shown in Fig. 1) during January and February over the period 1978–2025, yielding 2,796 days of data.

Air temperature is measured at a height of 1.5 m at most sites, although several sites use higher sensor heights (1.9–3.4 m). Preliminary tests showed that, for the sites included in the main analysis, most temperature sensors are installed at 1.5 m, and no systematic relationship was found between sensor height and the magnitude of nocturnal temperature drops. Accordingly, no height correction was applied.

In contrast, wind speed measurements required correction because sensor height changed at many sites during the study period. Wind speed was adjusted to a standard height of 10 m by assuming a logarithmic wind profile, with the aerodynamic roughness length fixed at 0.01 m for all sites.

For sites where sunshine duration instruments were replaced during the study period, bias corrections were applied following the Japan Meteorological Agency (2024). Sunshine duration observations were discontinued in March 2021 and replaced by satellite-derived estimates; these satellite-based values were used as observational data for subsequent years.

2.3. Definition of analytical variables

In this study, the nighttime period was defined as 16:00 to 07:00 on the following day (all times Japan Standard Time; JST), corresponding approximately to the interval from one hour before the mean sunset time to one hour after the mean sunrise time in Hokkaido during January and February. During this period, the net radiation at the surface typically becomes negative, indicating the onset and progression of nocturnal radiative cooling. The nocturnal temperature change was defined as

$$\Delta T = T_{07} - T_{16}, \qquad (1)$$

where T_{16} and T_{07} represent the temperatures at 16:00 and 07:00, respectively. The cumulative sunshine duration sd (h) from 12:00 on one day to 12:00 on the next day was used as a surrogate indicator of nighttime weather conditions. The mean wind speed over the 12-h period from 18:00 to 06:00 was defined as the nocturnal wind speed u_{n} (m s^{-1}). This averaging period was selected because it corresponds to the part of the diurnal cycle during which near-surface winds are typically weakest. Although nocturnal wind speed varies depending on weather conditions, the wind speed during clear nights serves as a key indicator of a site's susceptibility to strong radiative cooling. The representative clear-night wind speed was estimated as follows. First, the relationship between sunshine duration and the nocturnal wind speed u_{n} was quantified at each site using all data from the analysis period (see Fig. 6 for examples). Then, using the fitted regression line, the expected wind speed corresponding to a sunshine duration of 10 h was calculated and defined as the clear-night wind speed, u_{sd10} (m s^{-1}).

2.4. Principal component analysis of nocturnal temperature change

To identify the regions in Hokkaido where particularly strong nocturnal cooling frequently occurs, principal component analysis (PCA) was applied to nocturnal temperature changes. In this analysis, anomalies relative to the daily spatial mean across Hokkaido were used, rather than the more common long-term mean at individual sites (e.g., Maki and Harimaya, 1984). This approach enables the detection of areas where larger temperature drops occur more frequently and in a more synchronized manner compared with other regions within Hokkaido. Based on the spatial patterns of the two leading principal components, areas exhibiting large values were identified.

2.5. Criteria for identifying radiative-cooling nights

For each identified region, 20 representative sites were selected, and nights meeting meteorological conditions conducive to widespread substantial radiative cooling were selected based on the following criteria: (1) sunshine duration of at least 5.5 h and exceeding the normal value; (2) nocturnal wind speed below the normal value; (3) the magnitude of nocturnal temperature change exceeding the normal value; and (4) the 20-site average nocturnal temperature change falling below −10°C. Here, the normal value refers to the mean value calculated at each site over the entire analysis period. In addition, the threshold of 5.5 h used in the sunshine-duration criterion was selected after testing several candidate values, with the aim of improving the detection of radiative-cooling nights at sites located on the Sea of Japan side of Hokkaido, where sunshine-duration normals are generally low. Nights satisfying these criteria at 80% or more of the selected sites were identified as radiative-cooling nights.

2.6. Topography data

Digital elevation data from the 10-m mesh digital elevation model (DEM) provided by the Geospatial Information Authority of Japan were used to analyze the terrain surrounding each site. The terrain that influences nighttime surface air temperature is generally limited to the catchment, in which the site is located, because cold-air accumulation is constrained by local drainage pathways (Kondo and Okusa, 1990; Döscher *et al.*, 2023). Additionally, the influence of distant upstream terrain is unlikely to reach the site within a single night. In basins and similar landforms, cold-air inflow and CAP typically develop during the first half of the night (Clements *et al.*, 2003; Dorninger *et al.*, 2011), and representative speeds of cold-air drainage flows are on the order of 1 m s^{-1} (Kondo and Sato, 1988). Thus, the origin of cold-air drainage that affects the surface temperature at a given site can reasonably be assumed to lie within approximately 10 km upstream of the site. Based on this consideration, the primary analysis in this study focused on terrain within a 10-km radius of each site, restricted to the catchment in which the site is located. An example of the analyzed topography is shown in Fig. 2.

2.7. Algorithm for determining catchments

The catchment associated with each site was delineated using

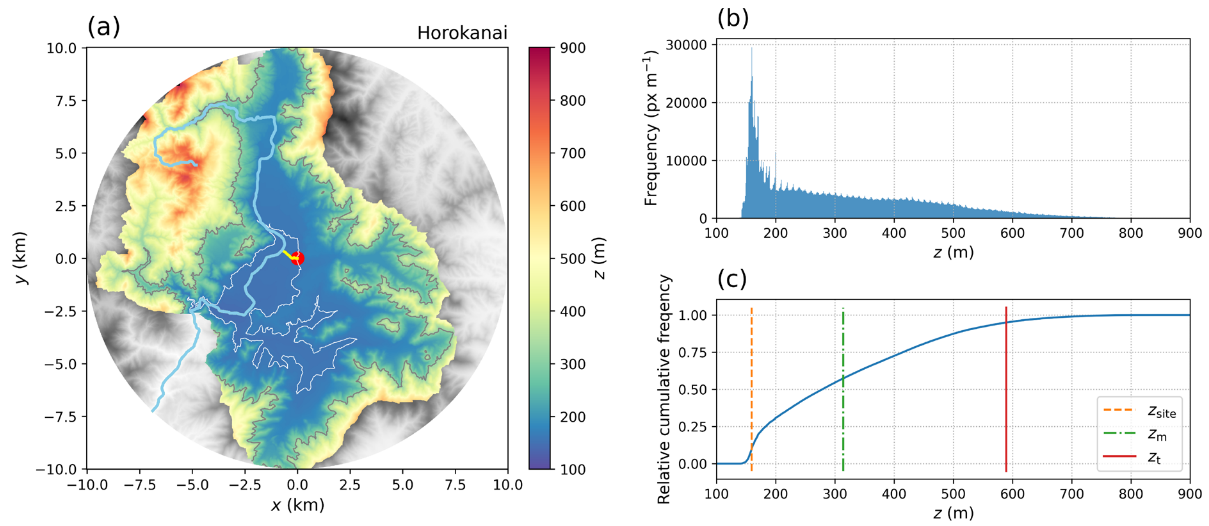

Fig. 2. Example of the analyzed topography at Horokanai (44° 0.6′ N, 142° 9.6′ E). (a) Elevation map of the delineated catchment. The red circle indicates the site location, and the sky-blue and yellow lines denote the main stream of the catchment and the drainage path from the site, respectively. Thin lines show the contours of the site elevation z_{site} (white) and the mean elevation z_m of the catchment (gray). (b) Elevation histogram. One pixel corresponds to an area of 10 × 10 m^2. (c) Relative cumulative frequency of elevation.

the following procedure.

1. Preprocessing of topography data
   A 20-km-radius DEM around each site was used to fill depressions and compute flow directions following Jenson and Domingue (1988). A larger domain than the final analysis area was used to minimize edge effects.
2. Clipping and flow-accumulation calculation
   The resulting flow-direction raster was clipped to a 10-km radius around the site, and flow accumulation (Jenson and Domingue, 1988) was then computed for all cells within this domain.
3. Identification of the main drainage path
   The flow path originating from the cell containing the site was traced using the flow-direction raster. The point at which this path exited the 10-km radius or reached the coastline was defined as the terminal outflow point. From this point, the main drainage path within the catchment was identified by tracing upstream along the direction of maximum flow accumulation.
4. Cross-sectional area of cold-air drainage
   Cross-sectional areas along the main drainage path were computed. Based on Kondo and Sato (1988), the thickness of down-valley flows with drainage distances shorter than 10 km is typically less than 50 m; therefore, the cross-sectional areas S_{out} were calculated using elevations from the channel bed up to 50 m above it.
5. Determination of the downstream boundary of the catchment
   Downstream of the confluence with the site's outflow path, the point at which the cross-sectional area satisfied S_{out} < 0.02 km^2 and reached its minimum value was defined as the downstream boundary. If no such point existed, the terminal outflow point was used as the boundary.
6. Catchment delineation
   Once the downstream boundary was determined, the contributing area draining to that point was delineated using the flow-direction raster. If the boundary coincided with the terminal outflow point, a base region was defined as the set of cells adjacent to the outflow point with elevations less than 10 m above the outflow-point elevation; the catchment was then defined as the set of higher-elevation cells connected to this base region.

All topographic analyses were performed using custom Python scripts.

2.8. Definition of topographic parameters

For each site, terrain characteristics within the delineated catchment were quantified using elevation data from the DEM. The 95th-percentile elevation was defined as the upper terrain height z_t (m), and the 1st-percentile elevation as the lower terrain height z_b (m). The mean elevation of the catchment within a 10-km radius was denoted as z_m (m). The area where elevation satisfies $z \le z_m$ was defined as the *inner region* of the catchment. The inner-region depth d_{in} (m) was defined as

$$d_{in}=z_m-z_b, \quad (2)$$

representing an approximate measure of the depth of the CAP layer. Following previous studies (Kondo and Okusa, 1990; Gustavsson *et al.*, 1998; Lindkvist *et al.*, 2000; Lundquist *et al.*, 2008; Kimura *et al.*, 2023), several topographic factors that may influence nocturnal temperature drop were evaluated:

A_t: total catchment area within a 10-km radius (km^2)
A_{in}: area of the inner-region terrain (km^2)
S_{out}: cross-sectional area of the catchment outlet (km^2)
Sh: shape parameter of the inner-region terrain (dimensionless), defined as $Sh=V_{in}/(A_{in}d_{in})$, where V_{in} (km^3) is the volume of air enclosed within the terrain below z_m

Site-specific parameters were also considered:

z_{site}: site elevation (m)
$z_{site}-z_b$: site relative elevation (m)
A_{site}: area within the catchment where $z \le z_{site}$ (km^2)

slp_{site}: mean terrain slope (°) within a 100-m radius of the site

A_{site}/A_{in}: fraction of the inner-region area lying below the site elevation (dimensionless)

To characterize the overall radiative-cooling capacity of the terrain envelope, we defined a new parameter:

$$R_{av} = \frac{A_t}{V_t}. \quad (3)$$

Here, V_t denotes the volume of air contained within the terrain between z_b and z_t. Larger values of R_{av} (km^{-1}) indicate more effective radiative losses across the plan-view area of the catchment relative to the volume of air enclosed by the terrain, thereby enhancing the net cooling (i.e., decreasing the mean temperature) of the atmosphere contained within the terrain.

These terrain-based parameters were treated as candidate explanatory variables for nocturnal temperature drop. For each analysis in Section 3.6, the most influential variables were selected through a two-step procedure:

1. multicollinearity screening using the variance inflation factor (VIF), removing variables with VIF ≥ 10; and
2. recursive feature elimination (RFE; Guyon *et al*., 2002) applied to the remaining variables using a linear regression model.

All statistical analyses were performed using Python, with VIF values computed using the statsmodels package and RFE implemented using the scikit-learn library.

3. Results and Discussion

3.1. Regional distribution of statistics over the entire analysis period

We first take a quick look at the regional distribution of temperature statistics calculated over the entire analysis period. Fig. 3(a, b) presents the spatial distribution of the mean and minimum values of the daily minimum temperature T_{min} throughout the analysis period. Rikubetsu (−19.2℃), Shimukappu (−17.8℃), and Nukanai (−17.7℃) exhibit the lowest mean T_{min}, while the lowest individual minimum temperatures were recorded at Etanbetsu (−38.1℃; 1978/02/17), Utanobori (−37.9℃; 1978/02/17), and Horokanai (−37.6℃; 1978/02/17). Overall, although the southeastern region shows lower mean minimum temperatures, the most extreme low temperatures tend to occur in the northern inland areas. In contrast, temperatures in the southwestern region are relatively high.

Fig. 3(c–f) presents statistics for the daily nocturnal temperature change ΔT, including the mean and minimum values, as well as the number of nights when ΔT fell below −10℃ or −20℃. The mean temperature drop (Fig. 3c) and the number of nights with typical magnitudes of nocturnal cooling (Fig. 3e) exhibit clear regional differences across Hokkaido, with smaller magnitudes on the Sea of Japan side and larger magnitudes on the Pacific side. The three sites with the lowest mean ΔT are Rikubetsu (−12.0℃), Ashoro (−11.1℃), and Nukanai (−11.1℃). In contrast, sites experiencing exceptionally large temperature drops (Fig. 3d) and those where such events occur frequently (Fig. 3f) are distributed throughout inland areas regardless of region, although a slight concentration is evident in northern Hokkaido. The largest individual temperature drops were recorded at Shimukappu (−28.4℃; 1986/01/21), Utanobori (−25.9℃; 2000/02/03), and Etanbetsu (−25.8℃; 1978/02/26).

3.2. Factors influencing the regional distribution of the long-term mean nocturnal temperature drop

Regional distributions of the mean sunshine duration and the clear-night wind speed are shown in Fig. 4. The spatial pattern of sunshine duration reflects the typical winter weather conditions experienced in Hokkaido, with frequent snowfall along the Sea of Japan side and predominantly clear skies along the Pacific side (see Section 2.1). Comparison of Figs. 3c and 4a reveals a clear regional correspondence between the prevalence of clear weather and the mean temperature drop. Wind speed during clear nights (Fig. 4b) also contributes to the regional variation in the mean temperature drop, although its influence is relatively weaker. In the southeastern region (Pacific side), where sunshine duration is long, the mean temperature drop is generally large, and within the same region, sites with lower nocturnal wind speed tend to exhibit a greater temperature drop. In contrast, at capes and remote islands where wind speeds remain persistently high even at night, the mean temperature drop is generally small regardless of sunshine duration. Consequently, the regional variation in the mean temperature drop can be largely explained by a linear combination of the mean sunshine duration and the clear-night wind speed (Fig. 5). In other words, the spatial distribution of the mean temperature drop reflects the frequency of meteorological conditions that enhance radiative cooling, jointly shaped by the large-scale topography that governs regional weather patterns and local topography that modulates nocturnal wind speeds.

3.3. Relationship between daily nocturnal temperature drop and meteorological conditions

Fig. 6 shows the relationship between sunshine duration, nocturnal mean wind speed, and nocturnal temperature drop for two representative sites (Nayoro in the northern region and Ashoro in the southeastern region) throughout the entire analysis period. As expected, large temperature drops occur primarily under conditions of longer-than-average sunshine duration and weaker-than-average wind speeds. Similar tendencies were observed at other sites not shown in the figure. However, as indicated by the regression lines, the relationship between sunshine duration and nocturnal wind speed varies among the sites. Fig. 7, which shows the regional distribution of the regression-line slope $d(\log u_n)/dsd$, indicates that these differences are related to topography. At most sites, nocturnal winds tend to weaken on clear nights, as expected in a stable surface layer formed by radiative cooling. In contrast, at valley sites (scattered plots in upland areas with positive values) and at some coastal sites, nocturnal winds tend to increase on clear nights. Inspection of nocturnal wind direction at these sites indicates that these winds are down-valley flows or land breezes associated with local topographic features. More notably, in the inland area of the southeastern region (i.e., the Tokachi Plain), a tendency for nocturnal wind speed to increase with sunshine duration is widely observed. This is attributable to a large-scale topographic effect: when strong northwesterly winds prevail under the synoptic pressure pattern typical of winter around

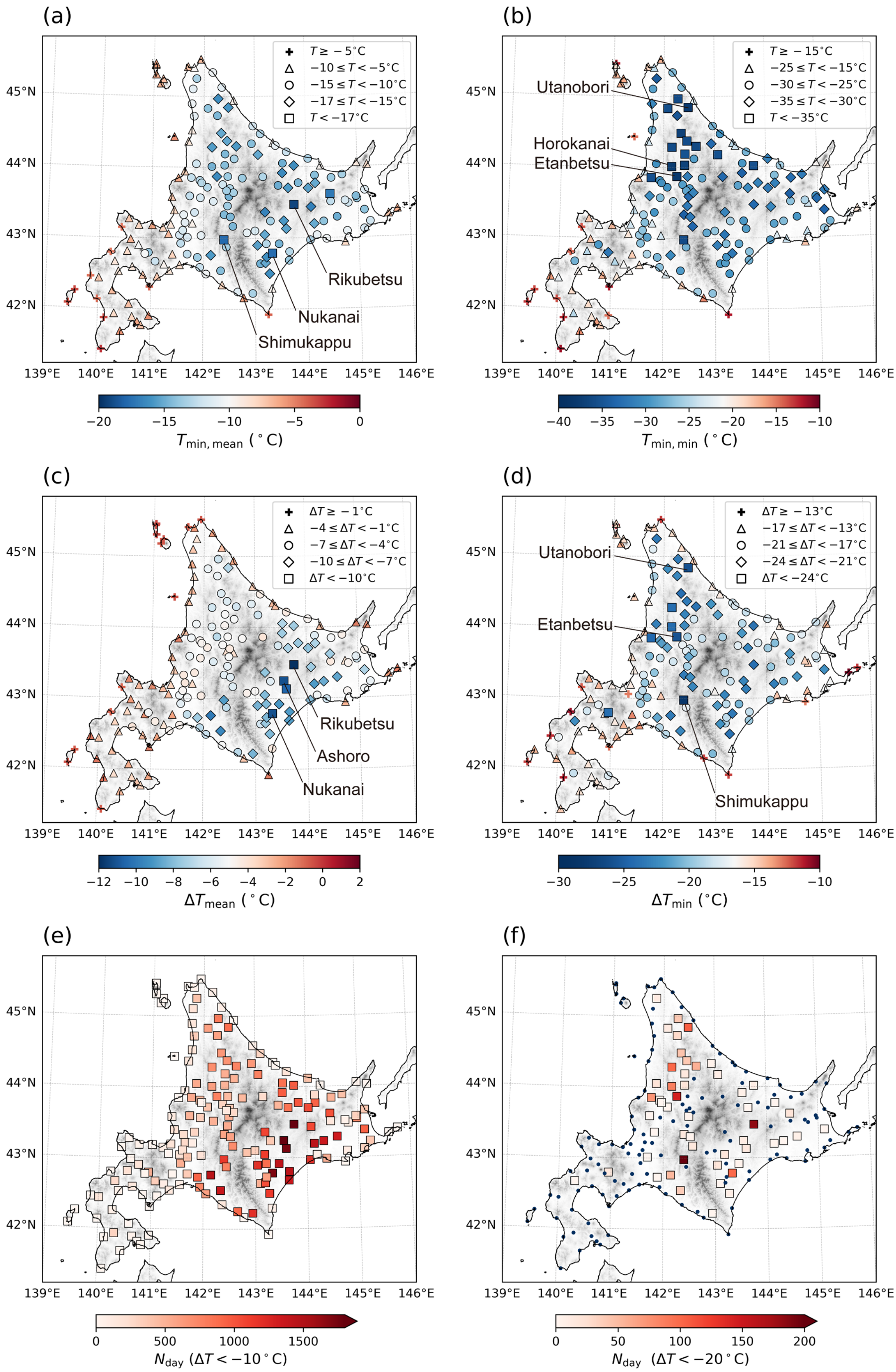

Fig. 3. Spatial distribution of temperature statistics calculated over the analysis period, showing (a) the mean and (b) the minimum values of the daily minimum temperature T_{min}; (c) the mean and (d) the minimum values of the daily nocturnal temperature change ΔT; and (e, f) the number of nights when ΔT fell below –10°C and –20°C, respectively.

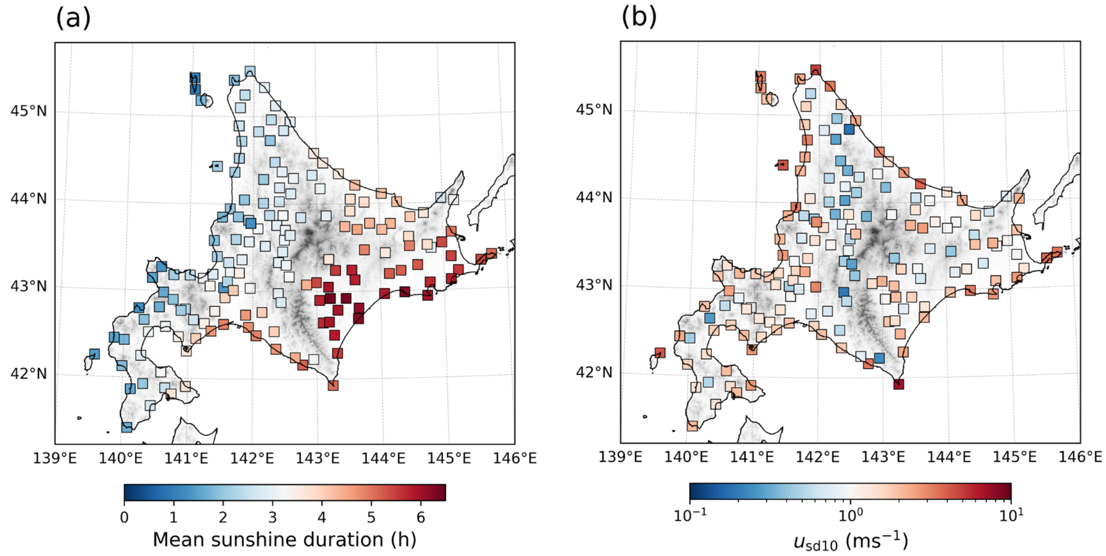

Fig. 4. Spatial distribution of (a) the mean sunshine duration and (b) the clear-night wind speed.

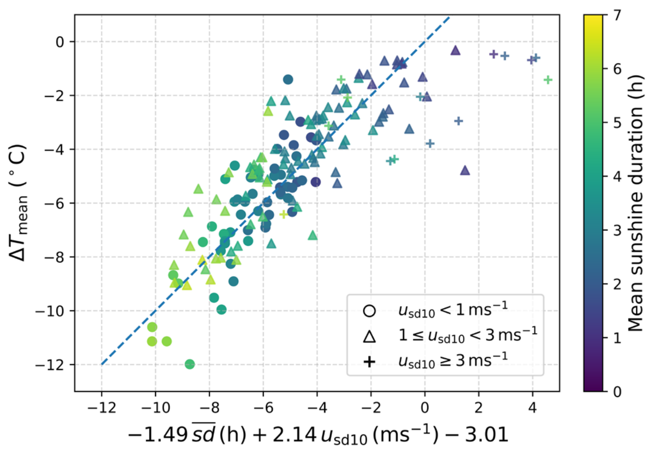

Fig. 5. Relationship between the mean sunshine duration $\overline{sd}$, the clear-night wind speed u_{sd10}, and the mean nocturnal temperature change ΔT_{mean} at all sites, based on the multilinear regression.

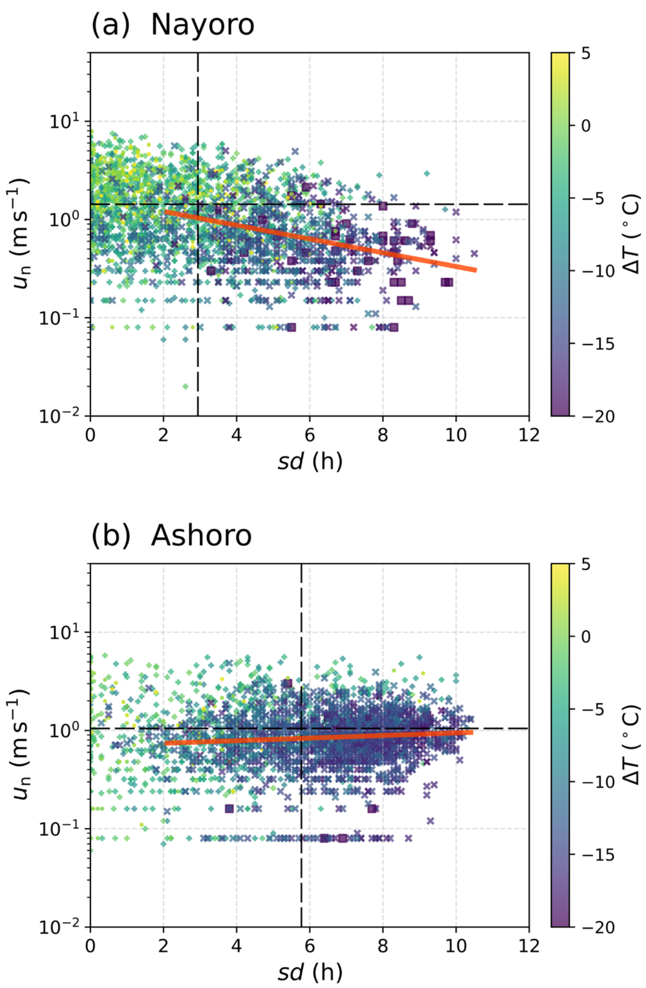

Fig. 6. Relationship between the daily sunshine duration sd and the nocturnal mean wind speed u_n throughout the analysis period for two representative sites: (a) Nayoro (44° 22.2′ N, 142° 27.4′ E) and (b) Ashoro (43° 14.6′ N, 143° 33.2′ E). Each plot is colored by the daily nocturnal temperature change ΔT. The horizontal and vertical long-dashed lines denote the mean values of u_n and sd, respectively. The bold red line represents the linear regression line evaluated for $2 \leq sd \leq 10$ h.

Japan, clear weather tends to occur on the leeward side of the mountain ranges.

Thus, the meteorological conditions that favor substantial nocturnal cooling differ systematically by region. In the following section, we identify those regions where large temperature drops are particularly likely and examine the intersite variability that emerges when radiative-cooling conditions develop within these regions.

3.4. Regional characteristics of substantial nocturnal temperature drops

As described in Section 2.4, principal component analysis of nocturnal temperature drops was conducted. Fig. 8 shows the spatial distributions of the resulting first principal component (PC1) and second principal component (PC2). PC1 exhibits large negative values in the southeastern region (Pacific side of Hokkaido), whereas PC2 shows large negative values in northern Hokkaido. Moreover, PC1 accounts for 46.3% of the total variance, and its spatial pattern closely resembles that of the mean sunshine duration (Fig. 4a). Although not shown here, the PC1 of sunshine duration exhibits a similarly structured spatial pattern (see Supplementary Fig. S1). These similarities suggest that the primary factor governing the distribution of substantial nocturnal cooling is the regional-scale weather pattern shaped by Hokkaido's large-scale topography (see Section 2.1). In contrast, although PC2 explains only 15.1% of the total variance, its distribution overlaps with regions where minimum temperatures are extremely low (Fig. 3b) and where particularly large temperature drops frequently occur (Fig. 3d, f). Clear nights are relatively infrequent in this region, but when they do occur, temperatures tend to drop substantially.

The cumulative contribution of the first two PCs exceeds 60%, and therefore these two regions (hereafter referred to as the "PC1 region" and the "PC2 region," respectively) are considered areas most likely to experience simultaneous and widespread nocturnal cooling. The top 20 sites with the largest negative values of PC1 and PC2 were selected for subsequent analyses. The selected sites are indicated by squares in Fig. 8, and a list of their locations, together with their mean and maximum temperature drops, is provided in the Supplementary material (Table S1). For context, three sites per region were also selected from remote islands and capes (indicated by triangles in Fig. 8) as reference sites minimally influenced by local topographic effects.

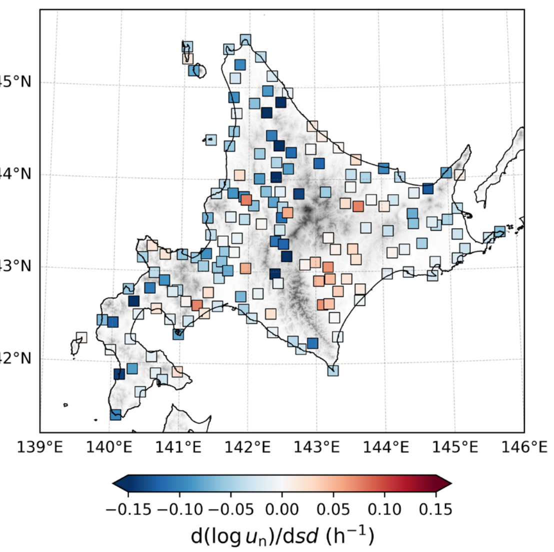

Fig. 7. Spatial distribution of the slope of the linear regression line between sunshine duration and the logarithm of the nocturnal mean wind speed.

3.5. Temperature changes at selected sites during radiative cooling nights

Based on the criteria described in Section 2.5, 75 nights in the PC1 region and 82 nights in the PC2 region were identified as radiative-cooling nights. Examination of the time series of temperature changes averaged over all radiative-cooling nights revealed that overnight temperature changes ranged from −18.8°C to −11.8°C in the PC1 region and from −20.0°C to −13.7°C in the PC2 region, whereas those at the reference sites were limited to less than 3°C (see Supplementary Fig. S2).

The criteria used to identify the radiative-cooling nights were based solely on local meteorological conditions, including substantial temperature drops. However, these conditions do not necessarily reflect the prevailing synoptic-scale atmospheric state. If many of the selected nights had been influenced by synoptic-scale cold-air advection, substantial temperature decreases would also have been observed at the reference sites. The fact that temperature changes at the reference sites remained sufficiently small indicates that synoptic-scale advection generally had only a minor influence on the selected nights. In addition, because the land surface in both the PC1 and PC2 regions is almost entirely snow-covered, differences in

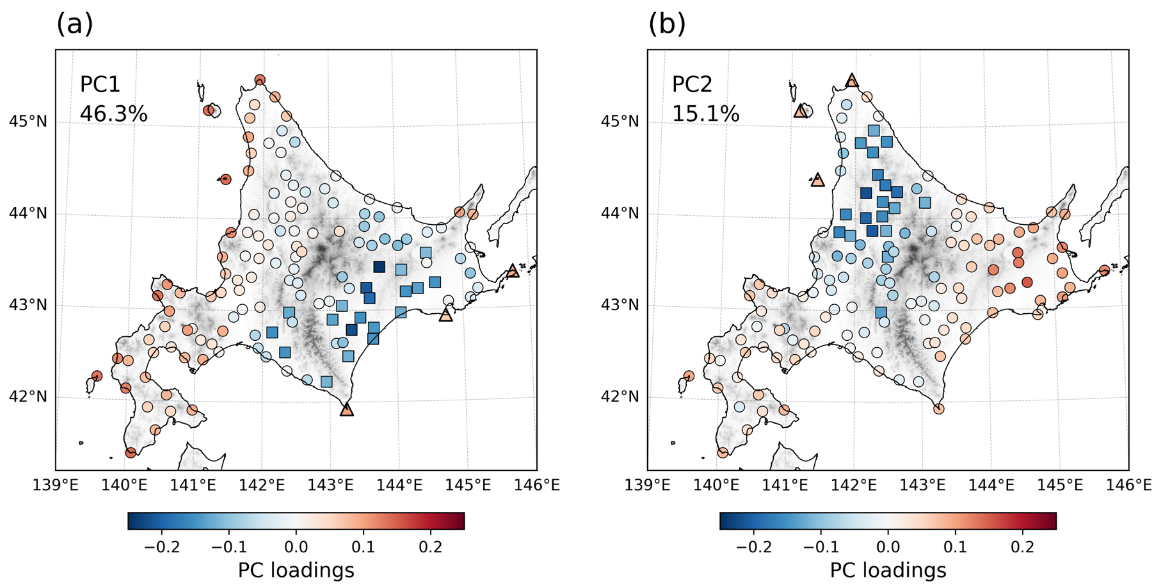

Fig. 8. Spatial distribution of the loadings of the principal components of nocturnal temperature changes: (a) PC1 and (b) PC2. Squares represent the top 20 sites with the largest negative values of the PCs, and triangles indicate the reference sites.

cooling rates due to land cover variability (e.g., Kusunoki and Ueno, 2022) are likely minimal. Thus, the observed temperature changes are expected to primarily reflect the influence of local topography at each site.

3.6. Topographic factors influencing temperature drops during radiative-cooling nights

Here, the topographic factors responsible for intersite variation in the mean nocturnal temperature drop, averaged over all the radiative-cooling nights, are examined separately for the two regions. In this section, we present the results of identifying the dominant influencing factors, and in the following section, we discuss their implications.

3.6.1. PC1 region – Southeastern Hokkaido

For the 20 representative sites selected within the PC1 region, multicollinearity among the candidate topographic parameters described in Section 2.8 was first assessed using VIF. After removing highly collinear variables, the remaining parameters were S_{out}, R_{av}, z_b, slp_{site}, $z_{site}-z_b$, and d_{in}. No statistically significant correlation (based on the Spearman's rank correlation coefficient) was found between any of these parameters and the mean temperature drop. Subsequent screening using the RFE method identified d_{in}, S_{out}, and z_b as statistically significant independent variables. However, multivariate linear regression using these variables did not adequately explain the intersite variability in temperature drop ($R^2 = 0.45$). Next, based on the variable with the largest regression coefficient, d_{in} (the inner-region depth), the sites were classified into three groups: (a) $d_{in} \geq 100$ m (deep terrain), (b) $50 \leq d_{in} < 100$ m (shallow terrain), and (c) $d_{in} < 50$ m (nearly flat terrain). The same screening procedure was applied to each group. The most influential variables identified were: (a) R_{av}, z_b; (b) R_{av}, S_{out}; and (c) R_{av}. Because all groups showed the strongest dependence on R_{av}, the mean temperature drop at each site was plotted against R_{av} (Fig. 9a). Across all groups, temperature drops tend to increase with R_{av}, with a stronger dependence observed in shallower-terrain groups. When comparing sites with similar R_{av}, deeper-terrain groups tend to exhibit larger temperature drop. However, within each group, the dependence on depth is not clearly evident, and cooling might even weaken as d_{in} increases.

3.6.2. PC2 region – Northern Hokkaido

First, to verify whether a similar relationship applies to the PC2 region, representative sites were classified by the inner-region depth, and the mean temperature drop was plotted against R_{av} (Fig. 9b). The topography spans only a narrow range of R_{av}, with most sites classified as deep terrain, yet substantial differences in temperature drop were observed. Thus, unlike the PC1 sites, neither R_{av} nor d_{in} explains the intersite variability.

Therefore, parameter screening was performed again for the PC2 region. Based on the multicollinearity assessment, S_{out}, slp_{site}, z_b, $\log_{10}(A_{site}/A_{in})$, and d_{in} were retained as independent variables. Subsequent screening using the RFE method identified $\log_{10}(A_{site}/A_{in})$ and z_b (in order of statistical significance) as significant variables. Fig. 10 shows the relationship between the mean temperature drop and $\log_{10}(A_{site}/A_{in})$. Although the scatter is large, a general tendency is apparent: the mean temperature drop increases as the fraction of the inner-region area lying below the site elevation decreases.

3.7. Interpretation of the relationship between topographic factors and temperature drop on radiative-cooling nights

At sites located within relatively shallow terrain (such as the shallow or nearly flat areas in the PC1 region), the mean temperature drop does not show clear dependence on other topographic parameters such as terrain depth or the shape parameter, despite their emphasis in previous studies (Kondo *et al*., 1989; Kondo and Okusa, 1990). In deep terrain such as basins, cold air produced by radiative cooling and sensible

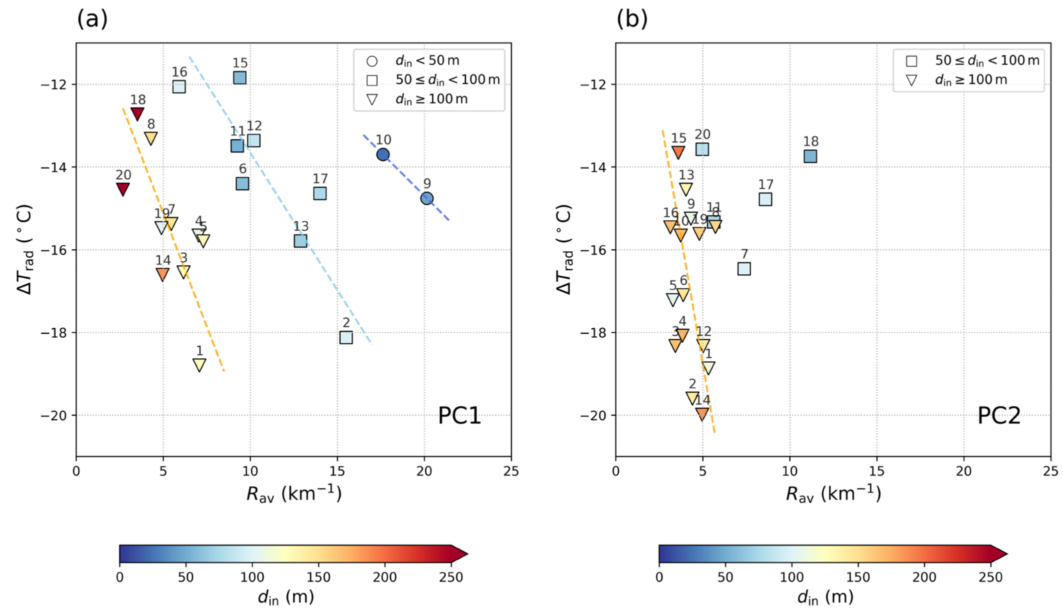

Fig. 9. Relationship between the area–volume ratio R_{av} of the terrain and the nocturnal temperature change averaged over all radiative-cooling nights (ΔT_{rad}) for the (a) PC1 and (b) PC2 regions. Broken lines represent the orthogonal distance regression lines for each inner-region-depth group, and the numbers near the plots indicate the sites according to their PC ranks (see Table S1).

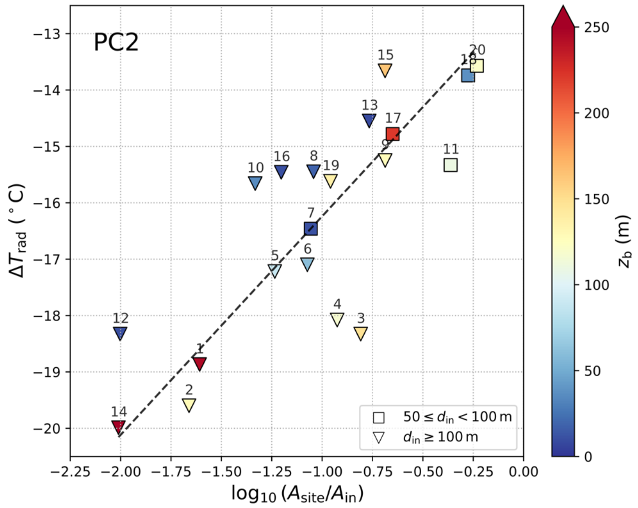

Fig. 10. Relationship between the fraction of the inner region area lying below the site elevation, A_{site}/A_{in}, and the nocturnal temperature change averaged over all radiative-cooling nights, ΔT_{rad}, for the PC2 region. The broken line represents the orthogonal distance regression line, and the numbers near the plots indicate the sites according to their PC ranks (see Table S1).

heat loss to the slope surface accumulates at the terrain bottom, thereby cooling the overlying air column to a considerable depth (Fig. 11a). However, in shallower terrain, the accumulation of cold air is inevitably limited. Additionally, as shown in Fig. 7, nocturnal winds in the PC1 region tend to strengthen under clear-sky conditions. These winds inhibit the stagnation and localization of cold air and enhance atmospheric mixing within the terrain (Fig. 11b). As a result, an isolated, decoupled inversion layer described below is less likely to form around the site (Vosper and Brown, 2008), and the surface air temperature tends to follow the temperature of the terrain-scale air mass more closely. Consequently, the magnitude of radiative cooling of the entire system−comprising the ground surface and the air mass within the terrain−is more directly reflected in the temperature drop observed at the surface. This provides a physical explanation for why temperature drops in relatively shallow terrain depend primarily on R_{av}, and why those in deep terrain within the PC1 region also show weak dependence on R_{av} (Fig. 9a).

However, when the terrain becomes sufficiently deep, the dependence of temperature drop on R_{av} decreases. This suggests that the radiative cooling of the entire system is not the dominant factor controlling the temperature drop near the terrain bottom, where most observation sites are located. Although the mean temperature drop of the entire atmosphere within the terrain should be determined by the total radiative energy loss overnight, this bulk cooling does not directly determine the temperature drop near the bottom of deep terrain. Cold-air currents flowing from surrounding slopes into the terrain bottom typically persist for 1–2 h after sunset, after which they intrude into the upper layer of the cold-air pool (e.g., Kondo *et al.*, 1983; Maki *et al.*, 1984; Whiteman *et al.*, 2010). As a result,

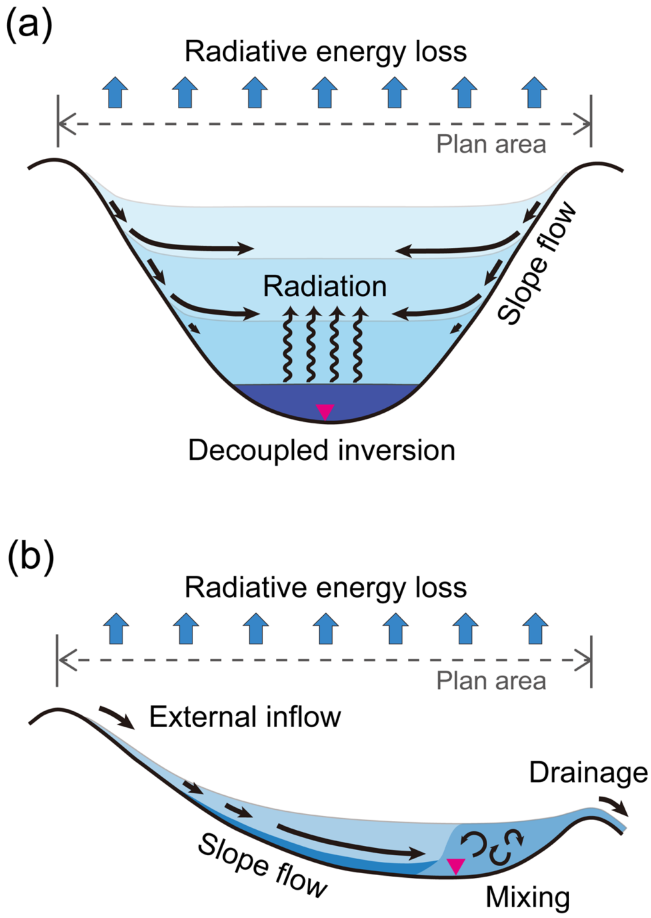

Fig. 11. Schematic illustration of the nocturnal cooling processes expected for (a) deep, closed terrain and (b) shallow or open terrain. The two terrains are assumed to have the same plan-view area, so their total radiative energy losses are approximately equal. The red inverted triangle indicates a typical location of the observation site.

the direct influence of radiatively cooled surrounding slopes on air temperature near the terrain bottom diminishes over time. Furthermore, on radiative-cooling nights, winds near the bottom of deep terrain weaken substantially as the cold-air pool develops, limiting turbulent heat exchange between the lowest part of the atmosphere and the ground surface. These progressive reductions in slope-driven advection and near-surface mixing cause the bottom-layer atmosphere to become increasingly thermally isolated and effectively decoupled from the overlying air (Sheridan *et al.*, 2014). Therefore, it is the local radiative cooling of this decoupled near-bottom atmosphere itself, rather than the radiative cooling of the entire terrain–atmosphere system, that becomes the dominant process governing nocturnal temperature drops at the deep-terrain site (Fig. 11a). This interpretation is consistent with previous studies that have noted the substantial contribution of *in situ* radiative cooling within intense surface-based inversions (Kondo *et al.*, 1978; Gustavsson *et al.*, 1998; Clements *et al.*, 2003). Under such conditions, detailed topographic features become less important, especially in closed terrain−consistent with observations by Whiteman *et al.* (2004), who reported minimal differences in temperature drops between sinkholes with different shapes.

However, the terrain surrounding observation sites is not always closed, even when it is deep. In open terrain, cold air can readily drain away from the surface (Fig. 11b). The resulting limited accumulation of cold air, together with enhanced turbulent mixing associated with drainage flows, reduces the magnitude of the nocturnal temperature drop. Even in terrain that is both deep and closed, the observation site may not be located at the terrain bottom where the cold-air pool is strongest (Fig. 10). These two factors introduce substantial variability in the local cooling environment and likely explain the variation in temperature drops observed among deep-terrain sites with similar R_{av} values (Fig. 9b).

Thus, the magnitude of the temperature drop depends strongly on the relative elevation of the observation site within the terrain and its position relative to the cold-air pool structure. To confirm these effects, Fig. 12 shows the mean temperature drop in the PC2 region plotted against the relative elevation $z_{site}-z_b$, with points colored by the cross-sectional outlet area S_{out}. As expected, large temperature drops occur at sites located near the local topographic minimum within closed terrain, characterized by small S_{out} values. In contrast, in open terrain with large S_{out}, temperature drops remain small regardless of the site's relative elevation.

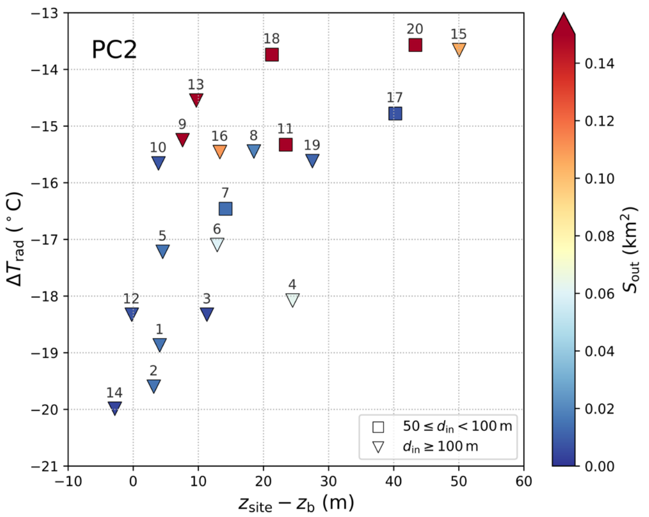

Fig. 12. Relationship between the relative site elevation, $z_{site}-z_b$, and the nocturnal temperature change averaged over all radiative-cooling nights, ΔT_{rad}, for the PC2 region. Color represents the cross-sectional outlet area S_{out}, and the numbers near the plots indicate the sites according to their PC ranks (see Table S1).

Open terrain often includes broad low-lying areas, which tend to yield large A_{site}/A_{in} values because observation sites are typically situated near the lower end of the elevation distribution. Thus, this parameter serves as an indicator of terrain openness. At the same time, the ratio also expresses the site's relative elevation within the terrain, since A_{site} represents the cumulative area with elevations lower than the site elevation (see Fig. 2). Accordingly, the combined influence of terrain openness and a site's relative elevation−both key controls on temperature drop in actual deep terrain−can be effectively summarized by this single parameter, as illustrated in Fig. 10. This framework provides a practical basis for identifying locations within complex terrain where extremely low temperatures are most likely to develop, offering a unified interpretation of how terrain geometry governs nocturnal cooling across diverse landscape types.

4. Conclusions

This study demonstrated that the regional characteristics of winter nocturnal temperature drops in Hokkaido are shaped by the combined effects of large-scale radiative conditions and local terrain-induced micrometeorological processes. Mean temperature drops exhibit a clear regional contrast, with stronger cooling on the Pacific side and weaker cooling on the Sea of Japan side. This contrast can be explained by the differing contributions of two factors: large-scale radiative conditions, captured by the sunshine duration during the 24-h noon-to-noon period, and the strength of local CAP, represented by the clear-night wind speed defined in this study. Principal component analysis further revealed that southeastern and northern Hokkaido are the regions most susceptible to substantial nocturnal cooling, with the former experiencing such events most frequently and the latter exhibiting the largest individual temperature drops.

A key contribution of this study is the introduction of the terrain-based metrics R_{av} and A_{site}/A_{in}, which together provide a mechanistic and generalizable framework for diagnosing nocturnal cooling potential across diverse landscapes. While deep, closed terrain favors strong cooling, consistent with previous studies, temperature drops in shallower terrain−common in southeastern Hokkaido−show weaker dependence on terrain depth or on the shape parameters used in earlier studies. Instead, they increase with the newly introduced parameter R_{av}, which represents the radiative-cooling efficiency of the terrain envelope. In deep terrain, the influence of R_{av} weakens, and temperature drops depend more strongly on terrain openness and the site's relative elevation within the cold-air pool, effectively summarized by A_{site}/A_{in}. These results clarify the distinct physical controls governing cooling at shallow versus deep terrain sites and highlight the broader applicability of the proposed metrics.

The implications of these findings span sectors with differing sensitivities to low temperatures. While strong nocturnal cooling poses a risk to agriculture and forestry, the same thermal environment can also provide operational advantages for certain types of infrastructure, such as facilities that benefit from naturally low ambient temperatures. Thus, the terrain-based metrics presented here may assist both in identifying locations vulnerable to damaging cold events and in pinpointing areas where cold conditions can be strategically utilized.

Despite these advances, the air temperature measured at any given site is influenced not only by the topographic factors considered here but also by additional elements such as land surface characteristics within the terrain (e.g., Yamazaki, 1995), the microenvironment in the vicinity of the site (e.g., Sugawara and Kondo, 2019), and the degree of urbanization (e.g., Arnfield, 2003). Consequently, conclusions drawn from observations at a limited number of stations inevitably involve some degree of uncertainty. Several directions for further research remain. Remote sensing could provide more continuous characterization of the spatial and temporal evolution of cold-air formation. Numerical modeling—such as large-eddy simulations or high-resolution mesoscale models—could clarify the relative contributions of radiative cooling, turbulent mixing, and cold-air drainage. Incorporating land surface characteristics, including vegetation, snow cover, and land use patterns, could further improve understanding of surface energy balance effects. Finally, linking the terrain-based indicators proposed here to both species-specific low-temperature tolerance and the operational requirements of cold-region infrastructure would further enhance their practical relevance across ecological, agricultural, and industrial applications.

Acknowledgments

We gratefully acknowledge the Japan Meteorological Agency (JMA) for providing the surface meteorological observations used in this study and the Geospatial Information Authority of Japan (GSI) for supplying the digital elevation model (DEM) data. These publicly available datasets made this research possible. We thank Tsuneo Kuwagata, Yasushi Ishigooka, Sachinobu Ishida, Keisuke Ono, Atsushi Maruyama, and Hiroki Ikawa for their insightful discussions during the Joint Research Program of the Institute of Low Temperature Science, Hokkaido University (Grant Number 23G008). We also thank James Buxton from Edanz (https://jp.edanz.com/ac) for English editing of an earlier draft of this manuscript. This publication was supported by JSPS KAKENHI (Grant Number 23HP2004).

References

Arnfield AJ, 2003: Two decades of urban climate research: a review of turbulence, exchanges of energy and water, and the urban heat island. *International Journal of Climatology* **23**, 1–26. https://doi.org/10.1002/joc.859

Chung U, Seo HH, Hwang KH, *et al*., 2006: Minimum temperature mapping over complex terrain by estimating cold air accumulation potential. *Agricultural and Forest Meteorology* **137**, 15–24. https://doi.org/10.1016/j.agrformet.2005.12.011

Clements CB, Whiteman CD, Horel JD, 2003: Cold-air-pool structure and evolution in a mountain basin: Peter Sinks, Utah. *Journal of Applied Meteorology* **42**, 752–768. https://doi.org/10.1175/1520-0450(2003)042<0752:CSAEIA>2.0.CO;2

Debnath A, Elangbam S, Pandey A, *et al*., 2024: The hidden dangers of winter: A brief review how cold stress affects cattle production. *International Journal of Veterinary Sciences and Animal Husbandry* **9**, 152–156.

Dorninger M, Whiteman CD, Bica B, *et al*., 2011: Meteorological events affecting cold-air pools in a small basin. *Journal of Applied Meteorology and Climatology* **50**, 2223–2234. https://doi.org/10.1175/2011JAMC2681.1

Döscher N, Ketzler G, Leuchner M, 2023: Localising and quantifying night-time cooling effects from sub-catchments in a mid-European low mountain area. *Theoretical and Applied Climatology* **151**, 1855–1870. https://doi.org/10.1007/s00704-023-04360-0

Flores F, Arriagada A, Donoso N, *et al*., 2020: Investigation of a nocturnal cold-air pool in a semiclosed basin located in the Atacama Desert. *Journal of Applied Meteorology and Climatology* **59**, 1953–1970. https://doi.org/10.1175/JAMC-D-19-0237.1

Gustavsson T, Karlsson M, Bogren J, *et al*., 1998: Development of temperature patterns during clear nights. *Journal of Applied Meteorology* **37**, 559–571. https://doi.org/10.1175/1520-0450(1998)037<0559:DOTPDC>2.0.CO;2

Guyon I, Weston J, Barnhill S, *et al*., 2002: Gene selection for cancer classification using support vector machines. *Machine Learning* **46**, 389–422. https://doi.org/10.1023/A:1012487302797

Hamada Y, Nagata T, Kubota H, *et al*., 2012: Study on a snow storage system in a renovated space. *Renewable Energy* **41**, 401–406. https://doi.org/10.1016/j.renene.2011.11.012

Hamada Y, Nakamura M, Kubota H, 2007: Field measurements and analyses for a hybrid system for snow storage/melting and air conditioning by using renewable energy. *Applied Energy* **84**, 117–134. https://doi.org/10.1016/j.apenergy.2006.07.002

Japan Meteorological Agency, 2024: *Guidelines for Meteorological Observation Statistics*. Japan Meteorological Agency, Tokyo, pp. 144 (in Japanese).

Jenson SK, Domingue JO, 1988: Extracting topographic structure from digital elevation data for geographic information-system analysis. *Photogrammetric Engineering and Remote Sensing* **54**, 1593–1600.

Kimura K, Maruyama A, Sasaki K, *et al*., 2023: Fine-scale mapping of daily minimum temperature in a cropland with complex terrains through the combination of a cold flow accumulation model with inversion strength. *Agricultural and Forest Meteorology* **329**, 109247. https://doi.org/10.1016/j.agrformet.2022.109247

Kimura M, Urano S, 2005: Distribution and regional classification of meteorological resources concerning natural cold energy in Hokkaido, Japan. *Journal of Agricultural Meteorology* **60**, 877–880. https://doi.org/10.2480/agrmet.877

Kimura M, Urano S, Okada K, *et al*., 2010: Study on utilization of cold energy from natural ice—ice-making efficiency of small ice containers stacked in a cold room. *Cold Regions Science and Technology* **60**, 146–153. https://doi.org/10.1016/j.coldregions.2009.08.011

Kondo J, Kanechika O, Yasuda N, 1978: Heat and momentum transfers under strong stability in the atmospheric surface layer. *Journal of the Atmospheric Sciences* **35**, 1012–1021. https://doi.org/10.1175/1520-0469(1978)035<1012:HAMTUS>2.0.CO;2

Kondo J, Kuwagata T, 1984: A relation between the depth of nocturnal stable layer (cold-air-pool) and the topographical depth of the basin. *Tenki* **31**, 727–737 (in Japanese). https://www.metsoc.jp/tenki/pdf/1984/1984_12_0727.pdf

Kondo J, Kuwagata T, Haginoya S, 1989: Heat budget analysis of nocturnal cooling and daytime heating in a basin. *Journal of the Atmospheric Sciences* **46**, 2917–2933. https://doi.org/10.1175/1520-0469(1989)046<2917:HBAONC>2.0.CO;2

Kondo J, Mori Y, Yasuda N, *et al*., 1983: The nocturnal stable layer “cold air lake” formed in the basin. *Tenki* **30**, 327–334 (in Japanese). https://www.metsoc.jp/tenki/pdf/1983/1983_07_0327.pdf

Kondo J, Okusa N, 1990: A simple numerical prediction model of nocturnal cooling in a basin with various topographic parameters. *Journal of Applied Meteorology and Climatology* **29**, 604–619. https://doi.org/10.1175/1520-0450(1990)029<0604:ASNPMO>2.0.CO;2

Kondo J, Sato T, 1988: A simple model of drainage flow on a slope. *Boundary-Layer Meteorology* **43**, 103–123. https://doi.org/10.1007/BF00153975

Kusunoki K, Ueno K, 2022: Development of a nocturnal temperature inversion in a small basin associated with leaf area ratio changes on the mountain slopes in central Japan.

Journal of the Meteorological Society of Japan **100**, 913–926. https://doi.org/10.2151/jmsj.2022-047

Lindkvist L, Gustavsson T, Bogren J, 2000: A frost assessment method for mountainous areas. *Agricultural and Forest Meteorology* **102**, 51–67. https://doi.org/10.1016/S0168-1923(99)00087-8

Lundquist JD, Pepin N, Rochford C, 2008: Automated algorithm for mapping regions of cold-air pooling in complex terrain. *Journal of Geophysical Research* **113**, D22107. https://doi.org/10.1029/2008JD009879

Maki M, Harimaya T, 1984: Spatial variations of nocturnal cooling on Hokkaido Island. *Geophysical Bulletin of Hokkaido University* **43**, 1–15 (in Japanese with English summary). https://doi.org/10.14943/gbhu.43.1

Maki M, Harimaya T, Kikuchi K, 1986: Heat budget studies on nocturnal cooling in a basin. *Journal of the Meteorological Society of Japan* **64**, 727–741. https://doi.org/10.2151/jmsj1965.64.5_727

Maki M, Harimaya T, Kikuchi K, *et al*., 1984: Process of nocturnal cooling in a land basin. *Geophysical Bulletin of Hokkaido University* **43**, 17–29 (in Japanese with English summary). https://doi.org/10.14943/gbhu.43.17

McKee TB, O'Neal RD, 1989: The role of valley geometry and energy budget in the formation of nocturnal valley winds. *Journal of Applied Meteorology* **28**, 445–456. https://doi.org/10.1175/1520-0450(1989)028<0445:TROVGA>2.0.CO;2

Sheridan PF, Vosper SB, Brown AR, 2014: Characteristics of cold pools observed in narrow valleys and dependence on external conditions. *Quarterly Journal of the Royal Meteorological Society* **140**, 715–728. https://doi.org/10.1002/qj.2159

Snyder RL, Melo-Abreu JP, 2005: *Frost protection: fundamentals, practice, and economics*. FAO, Rome, pp. 223.

Sugawara H, Kondo J, 2019: Microscale warming due to poor ventilation at surface observation stations. *Journal of Atmospheric and Oceanic Technology* **36**, 1237–1254. https://doi.org/10.1175/JTECH-D-18-0176.1

Tareen MSK, Zueter AF, Zolfagharroshan M, *et al*., 2024: Seasonal ground cold energy storage potential for data center cooling using thermosyphon: A comparative study of five cities in Canada for carbon footprint reduction. *Journal of Energy Storage* **84**, 111486. https://doi.org/10.1016/j.est.2024.111486

Thivierge MN, Bélanger G, Jégo G, *et al*., 2023: Perennial forages in cold-humid areas: adaptation and resilience-building strategies toward climate change. *Agronomy Journal* **115**, 1519–1542. https://doi.org/10.1002/agj2.21354

Tsuda K, Tano S, Ichino J, 2015: Using naturally cold air and snow for data center air-conditioning and humidity control. *Electrical Engineering in Japan* **190**, 45–58. https://doi.org/10.1002/eej.22455

Vosper SB, Brown AR, 2008: Numerical simulations of sheltering in valleys: the formation of nighttime cold-air pools. *Boundary-Layer Meteorology* **127**, 429–448. https://doi.org/10.1007/s10546-008-9272-3

Whiteman CD, Haiden T, Pospichal B, *et al*., 2004: Minimum temperatures, diurnal temperature ranges, and temperature inversions in limestone sinkholes of different sizes and shapes. *Journal of Applied Meteorology* **43**, 1224–1236. https://doi.org/10.1175/1520-0450(2004)043<1224:MTDTRA>2.0.CO;2

Whiteman CD, Hoch SW, Lehner M, *et al*., 2010: Nocturnal cold-air intrusions into a closed basin: observational evidence and conceptual model. *Journal of Applied Meteorology and Climatology* **49**, 1894–1905. https://doi.org/10.1175/2010JAMC2470.1

Yamazaki T, 1995: The Influence of Forests on Atmospheric Heating during the Snowmelt Season. *Journal of Applied Meteorology and Climatology* **34**, 511–519.

Yan C, Shi W, Li X, *et al*., 2016: A seasonal cold storage system based on separate type heat pipe for sustainable building cooling. *Renewable Energy* **85**, 880–889. https://doi.org/10.1016/j.renene.2015.07.023

Yazaki T, Fukushima H, Hirota T, *et al*., 2017: Winter nocturnal air temperature distribution for a mesoscale plain of a snow-covered region: field meteorological observations and numerical simulations. *Journal of Applied Meteorology and Climatology* **56**, 519–533. https://doi.org/10.1175/JAMC-D-16-0133.1

Zardi D, Whiteman CD, 2013: Diurnal mountain wind systems. In *Mountain Weather Research and Forecasting* (ed. by Chow F, De Wekker S, Snyder B). Springer, Dordrecht, pp. 35–119. https://doi.org/10.1007/978-94-007-4098-3_2